

Tidal energy fluxes and dissipation in the Chesapeake Bay

Liejun Zhong*, Ming Li

Horn Point Laboratory, University of Maryland Center for Environmental Science, P.O. Box 775, Cambridge, MD 21613, USA

Received 30 August 2005; received in revised form 16 January 2006; accepted 2 February 2006
Available online 4 April 2006

Abstract

Tidal energy flux and dissipation in the Chesapeake Bay are examined using a three-dimensional baroclinic model. The model currents are validated by a comparison with observed tidal current ellipses collected during previous field surveys. The model elevations are validated against sea-level records collected at tidal gauges. The baroclinic model produces more accurate predictions for sea-level heights and tidal currents than the tidal models which do not consider the effects of stratification. The averaged rms differences between the observed and modeled surface elevations are 3.4 cm for the M_2 constituent and 0.7 cm for the K_1 constituent. The averaged rms differences between the observed and modeled tidal current ellipses are 2.6, 2.1 cm s^{-1} , 5.1° and 21.7° for the semi-major, semi-minor axes, inclination and phase of the ellipses, respectively. The total amount of tidal energy flux entering the Bay mouth is found to be 188 MW, 88% of which is associated with the M_2 component. Dissipation of tidal energy is highly non-uniform in the Chesapeake Bay. 40% of the energy dissipation occurs in four topographic hotspots: the Bay mouth region around the headland of Delmarva Peninsula, the region near the Rappahannock sill, the constriction near the Bay Bridge and the constriction north of Baltimore.

© 2006 Elsevier Ltd. All rights reserved.

Keywords: Tidal currents; Energy flux; Energy dissipation; Numerical modeling; Chesapeake Bay

1. Introduction

Tidal currents are believed to provide the dominant mechanism for generating turbulent mixing in many estuaries. However, it is not clear if tidal mixing dominates in the Chesapeake Bay estuary since tidal currents there are relatively weak and range between 0.1 and 1 ms^{-1} (Carter and Pritchard, 1988). On the other hand, observations have suggested that wind is an important source of mechanic energy into the Bay (Wang, 1979a, b).

Since turbulent mixing generated in the tidally driven bottom boundary layer is very different from that produced in the wind-driven surface mixed layer, we need to compare wind and tidal forcing in the Chesapeake Bay and quantify their relative roles in estuarine dynamics. As a step towards achieving this goal, we shall calculate tidal energy flux entering the Bay and investigate the dissipation of tidal energy inside the Bay. A numerical model validated against tidal measurements can be used to carry out these calculations.

There have been routine tidal measurements in the Chesapeake Bay. Ten tide gauge stations are permanently installed in the Bay and provide continuous sea-level measurements over the past

*Corresponding author. Tel.: +1 410 221 8232;
fax: +1 410 221 8490.

E-mail address: lzhong@hpl.umces.edu (L. Zhong).

several decades. In addition, extensive tidal surveys were conducted during two previous periods: one between 1970 and 1974 and one between 1981 and 1983. Browne and Fisher (1988, hereafter BF) compiled data collected during these field surveys and constructed charts of tidal range and tidal currents for all major harmonics. Tide in the Chesapeake Bay has the characteristics of a reflected, damped Kelvin wave, with a larger tidal range on the eastern shore (e.g. Hicks, 1964; Carter and Pritchard, 1988). The mean tidal range decreases from 0.9 m at the Bay's entrance to a minimum of 0.3 m at Annapolis, then rises to 0.7 m at the head. Average tidal current amplitudes decrease from a maximum of 1.03 m s^{-1} at the mouth to a minimum of 0.13 m s^{-1} in the middle Bay, but increase to 0.59 m s^{-1} at Baltimore in the upper Bay. The continuous sea-level records and historical tidal surveys provide excellent data sets to test and validate the numerical tidal model.

Tidal models have been developed for the Chesapeake Bay, but their primary objective has been to predict sea levels around the Bay. Using a two-dimensional (2D) barotropic model, Spitz and Klinck (1998, hereafter SK) conducted tidal simulations in the Chesapeake Bay and developed a data-assimilation technique to improve tidal height predictions. They assimilated surface elevation data from tidal gauges and inferred the bottom drag coefficient. They found that the drag coefficient varies between 2.5×10^{-4} and 3.1×10^{-3} and displays a periodicity corresponding to the spring-neap tidal cycle. SK suggested that water-column stratification is a possible cause for the periodicity in the drag coefficient. Their hypothesis is physically plausible and suggests that a three-dimensional (3D) baroclinic model that includes the effects of stratification may do a better job in predicting tidal flows in the Chesapeake Bay. Tidal currents are usually harder to predict than tidal elevations and thus present a more stringent test of the numerical tidal model. Since SK's barotropic model did not predict the vertical variation of tidal currents, their depth-averaged currents could not be directly compared with the current-meter data collected at different sampling depths as reported in BF. Therefore, the modeled tidal currents have not yet been validated against observations in the Chesapeake Bay.

In this paper we shall use a 3D baroclinic model to simulate tidal flows in the Chesapeake Bay. In order to evaluate the model's predictive skill, we will

compare both tidal elevations and tidal currents against observations. Our objective is to calculate the tidal energy flux entering the Bay's mouth and estimate the tidal energy dissipation inside the Bay. Our work is also stimulated by recent tidal simulations in other coastal regions. For example, using a 3D prognostic, primitive equation model, Cummins and Oey (1997) carried out numerical simulations of tides off Northern British Columbia. They found that inclusion of baroclinic effects significantly improved the predictions of tidal current ellipses. Similarly, Cummins et al. (2000) found that the inclusion of stratification improves the representation of K_1 currents in a numerical model for the diurnal tides off Vancouver Island. He and Weisberg (2002) used a 3D model to simulate tides on the West Florida Shelf and validated their model results against sea-level and current measurements along the coastline and across the shelf. On a smaller scale, Sheng and Wang (2004) investigated tidal circulation and nonlinear tidal dynamics in Lunenburg Bay, Nova Scotia.

Following Munk's survey (1997), some recent tidal studies have been directed at understanding tidal energy dissipation in marginal seas. For example, Davies and Kwong (2000) calculated tidal energy fluxes and dissipation on the European continental shelf. Lavelle et al. (1988) investigated similar issues in the Puget Sound on the US West Coast. More recently, Foreman et al. (2004) used a data-assimilation technique to estimate M_2 tidal dissipation in coastal waters surrounding the Vancouver Island. In simulations of the Gulf of California, Carbajal and Backhaus (1998) found that the dissipation of tidal energy is concentrated in the area of the Colorado River delta and over the Salsipuedes Sill. Tinis and Pond (2001) found that the sill of Sechart Inlet, British Columbia is a site of major tidal energy dissipation in the fjord estuary. These investigations suggest that most of tidal energy may be dissipated around isolated topographic features rather than uniformly distributed across the bottom boundary layer. Thus it is timely to examine the spatial distribution of tidal energy dissipation in a coastal plain estuary such as the Chesapeake Bay. If turbulent mixing is concentrated around a few isolated topographic features, these sites will play a special role in controlling salt transport in the estuary.

The paper is organized as follows. Model configuration is described in Section 2. In Section 3 we will

compare the results between 2D barotropic and 3D baroclinic models and examine the effects of stratification on tidal prediction. In Section 4 we will present model predictions of tidal currents and compare them with observed tidal current ellipses at a number of stations in the Bay. We calculate tidal energy flux and estimate energy dissipation in Section 5. In Section 6 we summarize the main results and compare tidal energy flux with a simple estimate of wind energy flux.

2. Numerical model description

We have configured the Regional Ocean Modeling System (ROMS) for the Chesapeake Bay. Fig. 1 shows model's bathymetry and its horizontal grid system. The bathymetry is extracted from high-resolution Coastal Relief Model data archived at NOAA's National Geophysical Data Center. We have selected a model domain that includes the main stem of the Bay as well as eight major tributaries. The domain also includes a piece of the coastal ocean so that sea level height at the open

boundary can be prescribed using a coarse-resolution global tidal model. We have designed an orthogonal curvilinear coordinate system to follow the general orientation of the deep channel and the coastline of the main stem. The grid size is less than 1 km in the cross-channel direction and 2–3 km in the along-channel direction. The total number of grid points is 120×80 . A more detailed description of this numerical model can be found in Li et al. (2005).

When simulating tides in the Chesapeake Bay, we run both the 2D barotropic model and 3D baroclinic model in order to examine the effects of water-column stratification as hypothesized in SK. In the 2D model, the bottom stress is parameterized as a quadratic function of the depth-averaged current. In order to compare with SK's model results, we use the same drag coefficient formula as theirs, *i.e.*, the drag coefficient c_D is prescribed as $c_D = gC^{-2}$, $C = h^{\alpha}n^{-1}$ in which h is the undisturbed water depth, C is the Chezy coefficient, and constant parameters α , n are chosen to be $\frac{1}{6}$ and 0.02, respectively (cf., SK; Daily and Harleman, 1966).

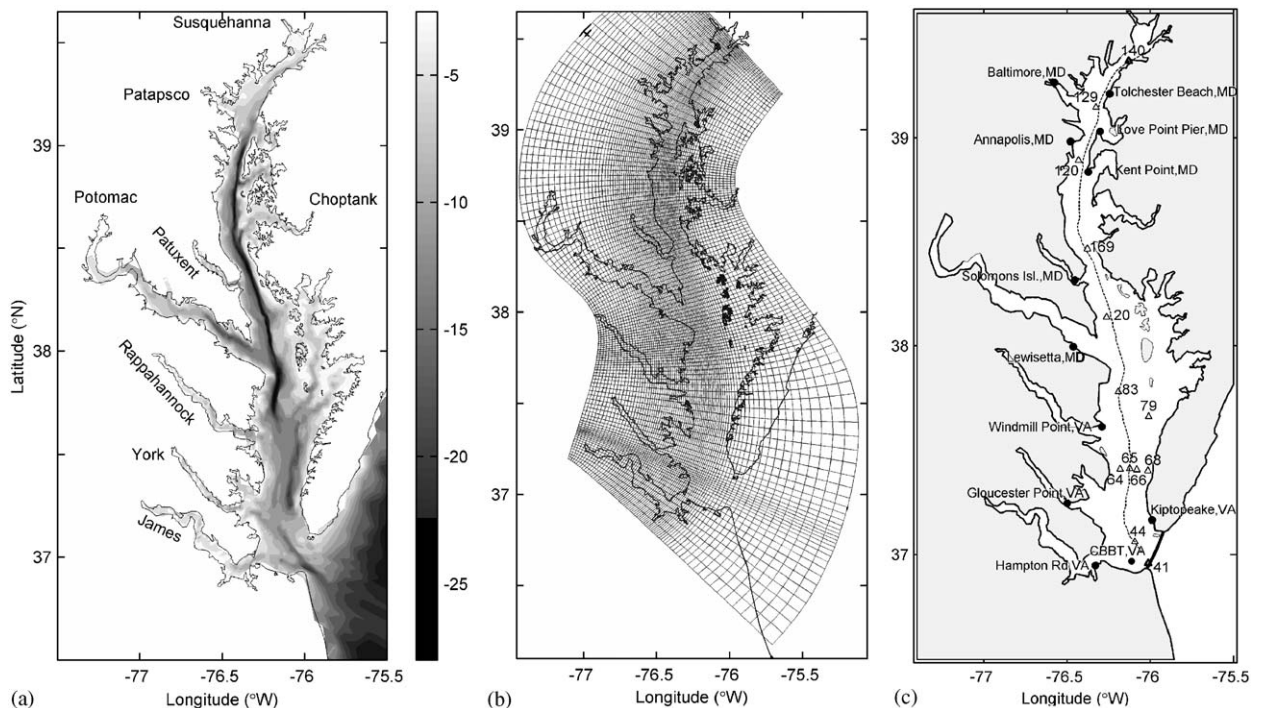


Fig. 1. (a) Bathymetry of the Chesapeake Bay and its adjacent coastal area. Major tributaries are marked. Depth scales are in units of meters. (b) A horizontal curvilinear coordinate system designed for resolving the complex coastlines and the deep channel in the Bay. The model has a horizontal resolution of about 1 km and 20 layers in the vertical direction. (c) Locations of tidal gauge stations (circles) and tidal-current measurement stations (triangles) used for the model-data comparison. The dashed line represents the centre axis of the main stem. The thick solid line at the Bay mouth represents the transect across which the incoming tidal energy flux is calculated.

This empirical formula links the flow resistance factor C to the drag coefficient. In our model, the minimum water depth is set to be 2.5 m and the corresponding drag coefficient is 0.0029. In the 3D model, 20 terrain-following layers are used in the vertical direction. The stretching parameters for the vertical grid are $\theta_s = 2$ and $\theta_b = 0.8$, as defined in the S-coordinate system (Song and Haidvogel, 1994). A quadratic stress is exerted at the bottom boundary, assuming that the bottom boundary layer is logarithmic with a bottom roughness height of 0.5 mm. Vertical eddy viscosity and diffusivity are computed using the Mellor–Yamada (or k–kl) turbulence parameterization scheme (Warner et al., 2005a). Coefficient of horizontal eddy viscosity and diffusivity are set to $1 \text{ m}^2 \text{ s}^{-1}$.

Tidal forcing at the open ocean boundary is specified using Oregon State University (OSU) global inverse tidal model of TPXO.6.2, which solves the Laplace tidal equations with a grid resolution of 0.25° by 0.25° and assimilates data from tidal gauge observations and TOPEX/Poseidon satellite measurements (Egbert et al., 1994; Egbert and Erofeeva, 2002). Tidal elevation at the open boundary is decomposed into five major tidal constituents, M_2 , S_2 , N_2 , K_1 , O_1 , using the harmonic constants linearly interpolated from OSU global tidal model. The open-ocean boundary condition consists of a Chapman's condition for surface elevation and a Flather's condition for barotropic velocity. In the 3D model, an Orlanski's type radiation condition is used for baroclinic velocity, and a combination of radiation condition and nudging (with a relaxation time scale of 1 day) are specified for temperature and salinity. Salinity and temperature fields on the offshore open boundary are prescribed using monthly Levitus climatology (Levitus, 1982) combined with field data at Duck,

North Carolina, acquired by the Field Research Facility of the US Army Corps of Engineers. At the upstream boundary in each tributary, daily freshwater inflow with zero salinity and time-varying temperature is prescribed according to observations. On each inflow cross section, the incoming current is uniform with time-varying speeds regulated by daily freshwater discharge rate. The Chapman radiation condition is used to filter out the outgoing tidal waves at the upstream boundary of each tributary.

Both the 2D and 3D models start from a state of rest with water surface at the mean sea level. The initial temperature and salinity distributions were obtained from a model run using the observed forcing for the year of 1995. The 3D model is then integrated for 160 days in 1996 until the salinity and temperature distributions reach a representative stratification condition. We have selected the following 58 days (between Julian day 160 and 218) for the analysis of tidal simulation results since 58-day gives an integer number of periods for each of the major constituents. Fig. 2 shows the salinity distribution in the along-channel section aligned with the center axis of the Bay. The salinity distribution is averaged over the 58-day period. This corresponds to the dry time between mid-June and mid-August so that the salinity distribution did not change much over this period. Li et al. (2005) provided a detailed comparison between the observed and predicted salinity distributions and found that the hydrodynamic model shows good skills in predicting salinity. We shall use the least-square error method by Pawlowicz et al. (2002) to calculate harmonic constants for individual tidal constituents. The same Matlab program is used to analyze tidal current vectors expressed in terms of an orthogonal scalar component pair and to

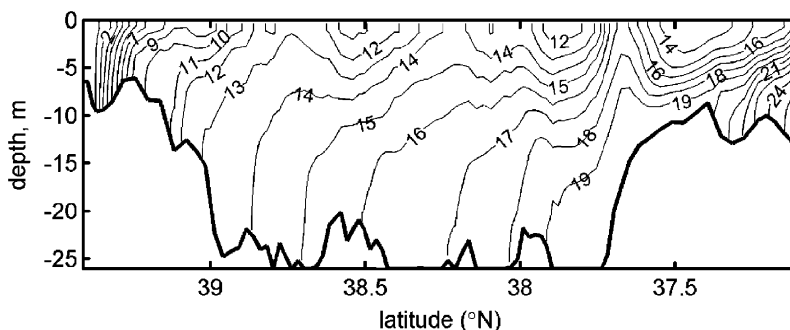


Fig. 2. Averaged salinity distribution in the along channel section aligned with the center axis of the Chesapeake Bay.

calculate parameters such as the semi-major, semi-minor axes and orientation of tidal current ellipses and the phase of tidal currents.

3. Effect of stratification on tidal prediction

In their 2D data-assimilation experiments, SK found that the drag coefficient fluctuated over the spring-neap cycle. The drag coefficient at neap tide was twice as much as that at spring tide. They suggested that stratification may be a cause for this periodic variation of the drag coefficient. To test this hypothesis, we shall carry out parallel simulations using a 2D barotropic model (hereafter 2D) and a 3D baroclinic model which incorporates the effects of stratification (hereafter 3Ds). For comparison, we will also present results from a 3D model in which water is unstratified or has constant density everywhere (hereafter 3Du).

To evaluate these tidal models, we shall compare the model results with sea level records obtained at tidal gauge stations in the Bay. These stations are a part of the National Tide and Water Level Observation Network and are maintained by National Oceanic and Atmospheric Administration (NOAA). We conducted harmonic analysis of observed water-level records at each tidal station and constructed surface-elevation time series using the harmonic constants of the five major tidal constituents M_2 , S_2 , N_2 , K_1 and O_1 . In this way we excluded sea-level fluctuations due to wind. The same harmonic analysis was applied to the predicted sea levels so that components such as Z_0 , M_4 , M_6 and MS_4 were excluded. In Fig. 3 we compare the observed and predicted (from 3Ds model) sea-surface elevations at six tidal stations in the Chesapeake Bay. Tochester Beach and Annapolis stations are in the upper Bay, Solomons Island and Lewisetta stations in the middle Bay, Windmill Point and CBBT in the lower Bay (see Fig. 1c for their locations). The modeled tidal elevations follow closely the observed records at the lower and middle Bay stations, but the model slightly overpredicted the tidal amplitude at the Tochester Beach station in the upper Bay.

A number of statistical measures have been used to quantify the predictive skill of the tidal models. Appendix A gives their mathematical definitions. Fig. 4 provides a summary for the range of the root-mean-square error, relative average error, correlation coefficient and the skill parameter for the 58-day analysis period. We have analyzed a total of

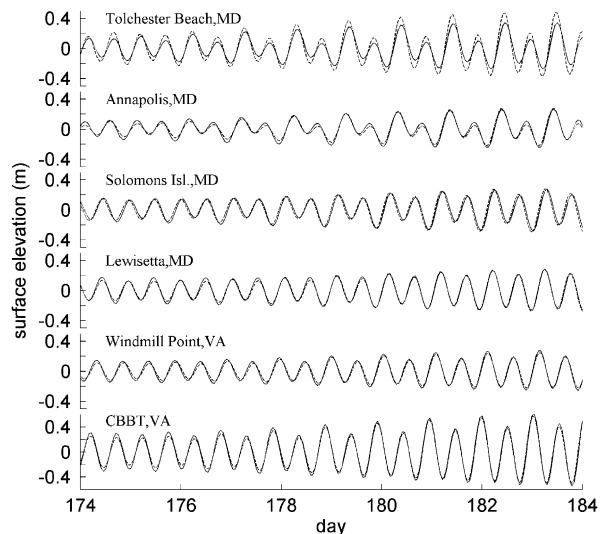


Fig. 3. Time series of observed (solid line) and modeled (dotted line) surface elevation at six tide gauge stations. Note the vertical scale is from -0.6 to 0.6 m for CBBT, VA station, and from -0.5 to 0.5 m for other stations.

12 tidal stations. At each station, we conduct a cross-comparison between 2D, 3Du (3D unstratified) and 3Ds (3D stratified) models. First we note that all three tidal models do a reasonable job in reproducing observed sea levels. Secondly, we note that the rms errors in 2D and 3Du models are almost identical except at the two upper Bay stations and at the station near Hampton Road, V.A. 3Ds model consistently performs better than the other two models: smaller rms and relative-average errors but higher correlation coefficients and skill scores. Therefore, the incorporation of stratification effects indeed improves the tidal-height prediction, as suggested in SK.

Besides the time-series analysis, we have conducted harmonics analysis and examined error statistics for each tidal component. Table 1 shows the observed and predicted M_2 and K_1 amplitudes and phases at the tide gauge stations. For the M_2 constituent, the 3Ds model has a smaller error than the 2D model except at the two upper Bay stations (Baltimore and Tochester Beach stations). We suspect that the 3Ds model may underestimate bottom friction in the shallow upper Bay regions and produce a larger reflected tidal wave from the upstream boundary, but the drag coefficient used in the 2D model takes the effect of water depth into account. When averaged over the 12 stations, the rms error D is 3.4 cm in the 3Ds model versus 4.2 cm

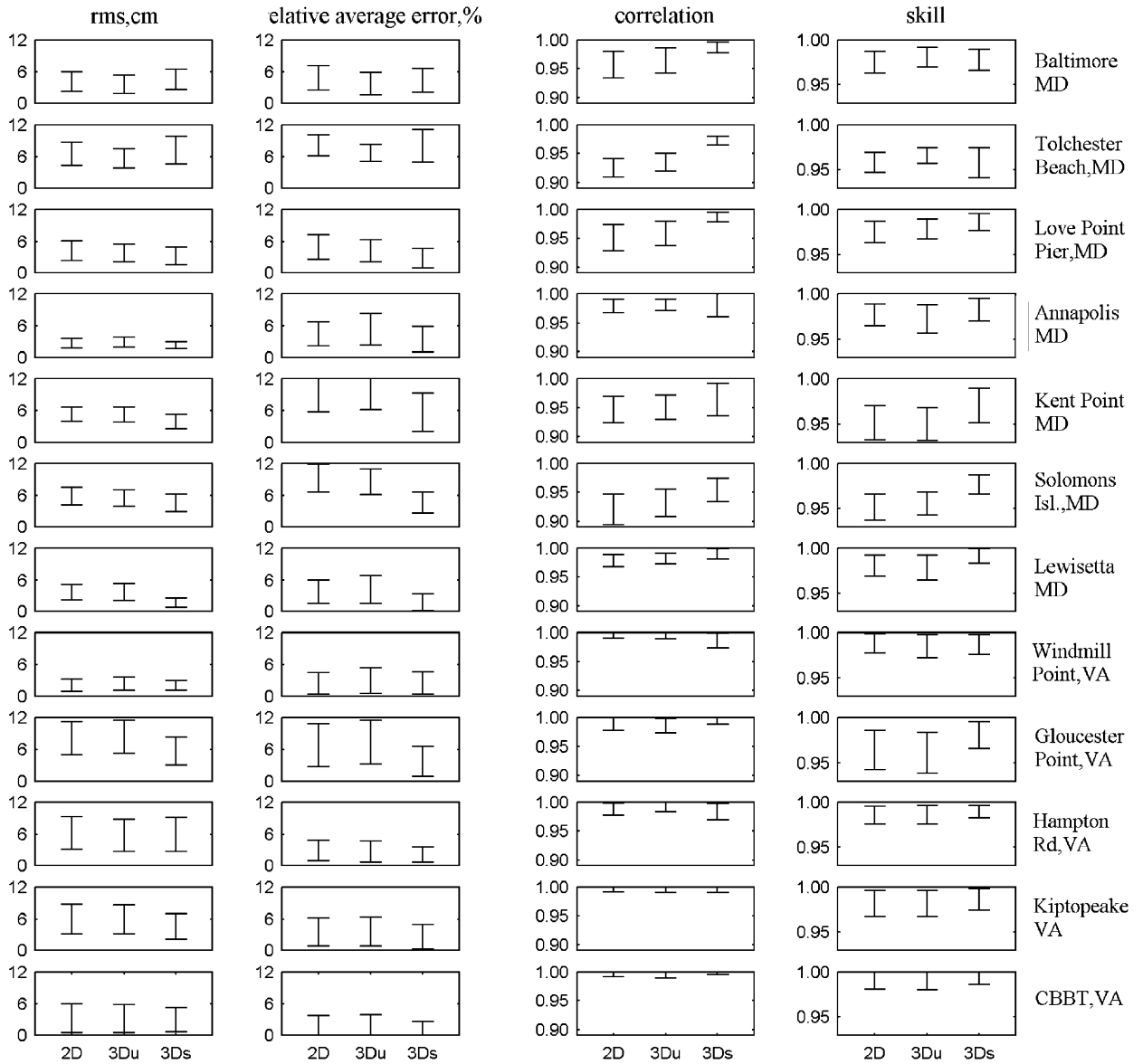


Fig. 4. Range of the root-mean-square error, relative average error, correlation coefficient and skill at 12 tide gauge stations for 2D barotropic and two 3D simulations. 3Ds includes stratification and 3Du assumes uniform density everywhere.

in the 2D model. For the K_1 constituent, the averaged rms error is 0.7 cm in the 3Ds model versus 0.9 cm in the 2D model. These error analyses confirm that the 3D baroclinic model provides a better prediction for individual tidal constituents.

We can look at spatial distributions of the tide in the Chesapeake Bay. Using surface-elevation time series obtained from the 3Ds model, we retrieved tidal amplitude and tidal phase at every water grid of the model domain. We focus on the two most important harmonics: semidiurnal M_2 and diurnal

K_1 constituents. Other constituents are relatively small: for example, the amplitudes of S_2 and N_2 constituents are about 10% and 20% of M_2 , respectively. Fig. 5 shows the co-amplitude and co-phase charts of M_2 constituent. The amplitude decreases from about 0.4 m at the entrance to a minimum of about 0.12 m in the middle Bay, then rises to 0.4 m at the head of the estuary. Due to the effects of Coriolis force, the amplitude is larger on the eastern shore than that on the western shore. There are two minima in the co-amplitude chart in

Table 1

Comparison of observed and modeled elevation amplitudes and phase lags, and root-mean-square error (D) for M_2 and K_1 at the tide gauge stations (see Fig. 1c for the locations)

Tide gauge	Amplitude (cm)			Phase (degree)			D (cm)	
	Obs	3Ds	2D	Obs	3Ds	2D	3Ds	2D
M_2								
Baltimore	17.0	22.9	19.8	147.7	145.0	134.2	4.2	3.6
Tolchester Beach	18.3	26.9	22.4	157.1	146.3	136.2	6.8	5.9
Love Point Pier	18.2	21.8	19.0	133.8	130.7	118.9	2.6	3.5
Annapolis	14.5	12.7	12.4	103.4	105.9	97.7	1.3	1.8
Kent Point	16.8	13.8	13.1	79.0	67.1	61.4	3.1	4.2
Solomons Island	18.3	18.9	16.0	9.5	7.5	13.0	3.9	5.0
Lewisetta	19.6	19.2	16.7	347.0	346.3	338.2	0.3	2.8
Windmill Point	18.0	16.5	15.3	273.4	279.9	274.9	1.7	1.9
Gloucester Point	36.8	29.1	26.2	222.5	225.4	228.2	5.6	7.8
Hampton Rd	36.8	34.6	31.2	215.7	206.0	208.3	4.5	5.0
Kiptopeake	40.9	34.5	32.7	203.1	205.4	204.4	4.7	5.9
CBBT	38.9	35.7	34.3	190.4	189.4	191.4	2.4	3.3
K_1								
Baltimore	7.5	8.4	6.2	161.0	155.8	151.8	0.8	1.2
Tolchester Beach	7.3	8.7	6.4	157.6	154.6	151.2	1.0	0.8
Love Point Pier	7.7	8.3	6.1	156.8	150.1	145.9	0.8	1.5
Annapolis	6.5	7.2	5.4	152.1	147.0	133.0	0.7	1.2
Kent Point	6.4	6.7	5.0	143.6	138.3	133.0	0.5	1.2
Solomons Island	4.5	3.7	3.1	119.8	121.4	112.2	0.6	1.0
Lewisetta	3.3	2.4	2.4	101.7	98.0	90.3	0.6	0.7
Windmill Point	2.8	2.2	2.2	46.9	33.0	38.2	0.6	0.5
Gloucester Point	5.1	4.1	3.9	2.0	0.2	7.4	0.7	0.9
Hampton Rd	5.0	5.3	5.1	8.0	6.4	0.2	0.9	0.5
Kiptopeake	5.9	5.7	5.5	3.4	3.2	3.0	0.5	0.5
CBBT	5.5	5.8	5.9	347.2	346.2	350.0	0.3	0.3

Obs stands for observations, 2D for a barotropic model and 3Ds for a 3D baroclinic model that includes stratification.

Fig. 5a. One is at the mouth of Potomac River and the other is at 38.9°N near Annapolis. These minima can be regarded as virtual amphidromes (BF, SK) and resulted from the interactions between the incoming and reflected waves. As shown in the co-phase lines, it takes about 14 hours for the M_2 tidal wave to travel from the Bay mouth to the head. Hence the Chesapeake Bay is able to hold a complete semidiurnal tidal wave at all times. The predicted co-amplitude and co-phase charts for the M_2 harmonics are in good agreements with those constructed from tidal gauges (see BF).

Next we examine K_1 constituent, the largest diurnal tidal component. The predicted co-amplitude and co-phase charts are shown in Fig. 6, which are also in good agreement with those tidal gauges (BF). The pattern of K_1 co-amplitude lines looks similar to that of M_2 tide; however, the K_1 amplitude is significantly smaller than M_2 tide. The ratio of K_1 amplitude to M_2 amplitude remains

about the same from the Bay entrance to the Patuxent River, but increases as the head of Bay is approached. This suggests that the relative contribution of K_1 to the total tide is greater in the upper Bay than in the lower Bay. One virtual amphidrome is also evident at the mouth of Potomac River in the K_1 co-amplitude chart and was reported in BF.

4. Comparison of tidal current ellipses with observations

Tidal currents are more variable and harder to predict than tidal heights since they are sensitive to bathymetric changes. In this section we shall compare predicted tidal currents with current-meter data collected during the experiment in 1981–1983 (BF). We assume the stratification condition simulated in our model is representative of those experienced during the research cruises.

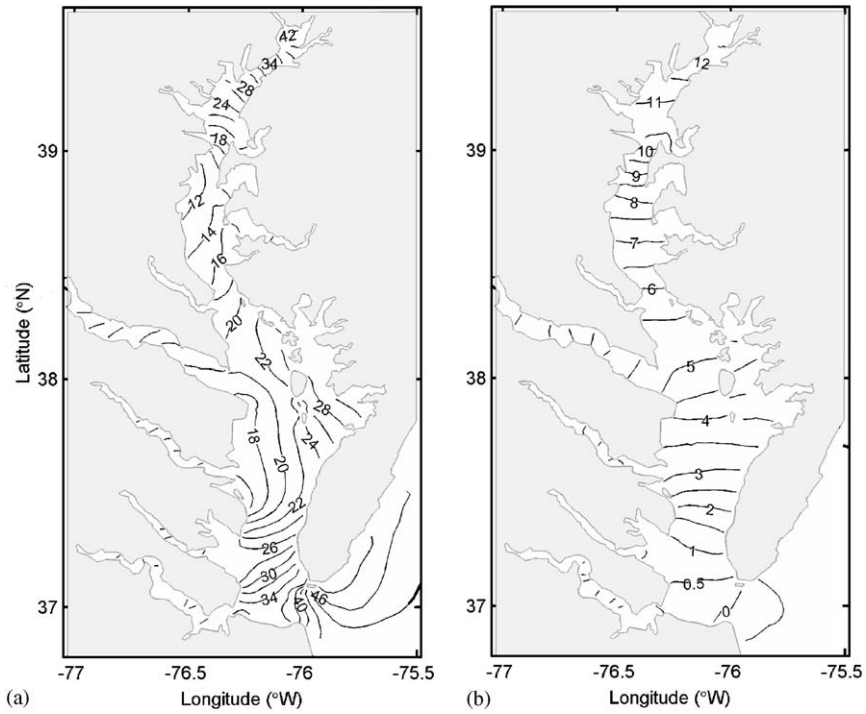


Fig. 5. Model predicted co-amplitude in cm (a) and co-phase in hour (b) for the principal semidiurnal M_2 tide.

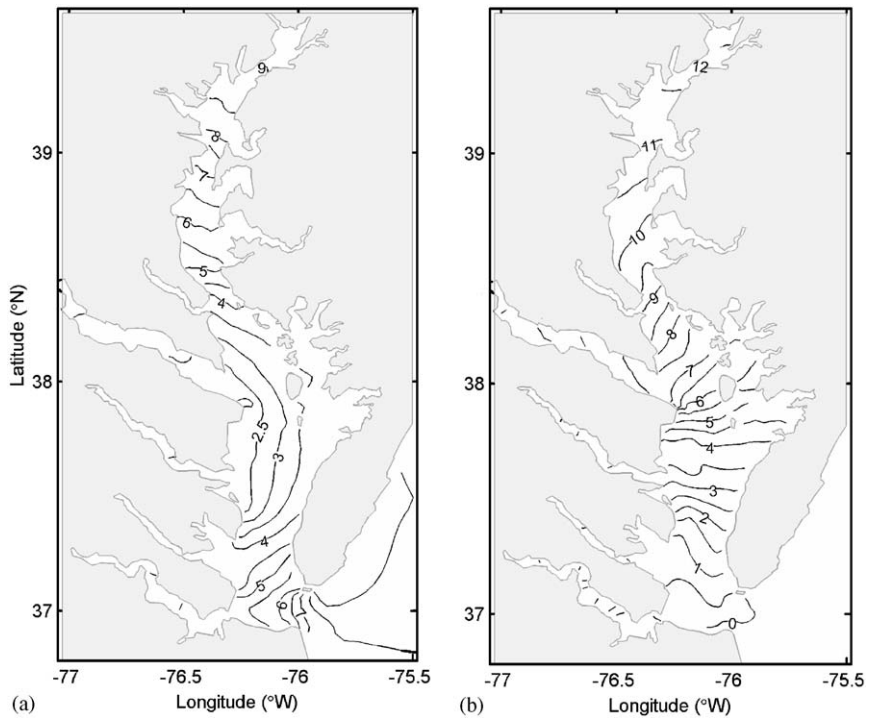


Fig. 6. Model predicted co-amplitude in cm (a) and co-phase in hour (b) for the principal diurnal K_1 tide.

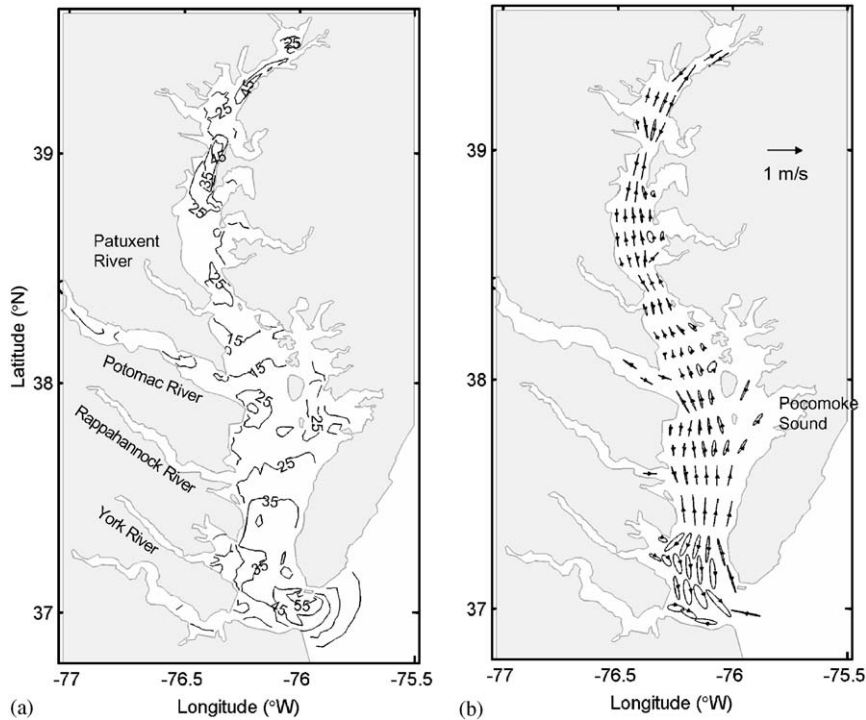


Fig. 7. (a) Model predicted co-amplitude of the M_2 tidal current (in cm s^{-1}). (b) Model predicted depth-averaged M_2 current ellipses.

Since M_2 is the dominant tidal harmonic, we shall focus on currents associated with this component. In Fig. 7a, we show the co-amplitude lines of the M_2 current. It has a maximum speed of 0.55 m s^{-1} at the Bay's entrance but decreases steadily within the lower reaches of the Bay, reaching a minimum value of 0.15 m s^{-1} just south of the mouth of the Patuxent River. Over the middle reach of the Bay, the current amplitude varies between 0.15 and 0.45 m s^{-1} , with lower values occurring in the wider cross sections and higher values in the narrower cross sections. The current speed at the Chesapeake Bay Bridge is about 0.45 m s^{-1} but is reduced to about 0.25 m s^{-1} at the head of the estuary. Fig. 7b shows the distributions of tidal current ellipses for the depth-averaged velocity associated with the M_2 constituent. Large clockwise-rotating ellipses with relatively large eccentricity (ratio of semiminor to semimajor axis) are found in the lower Bay (up to the mid-point between York River and Rappahannock River) where the coastlines show an abrupt change in their orientation. Tidal ellipses with smaller eccentricity are found in the Pocomoke sound area (lying between the latitudes at the Rappahannock River and Potomac River) where the Bay is wide. Elsewhere in the main stem of the

Chesapeake Bay, however, the tidal ellipses collapse onto straight lines. The channel boundaries constrain the tidal motions to be nearly rectilinear, aligned along the centre axis of the Bay.

An extensive Chesapeake Bay Circulation Survey was conducted by the National Ocean Services (NOS) from August 1981 through December 1983, during which tidal currents in the Chesapeake Bay were measured. We have chosen 10 representative current-meter stations along the center-axis of the main stem for the model-data comparison (see Fig. 1c for their locations). Fig. 8 compares the M_2 current ellipses at 5 m depth between the observations and those predicted from 3Ds and 3Du models.

The observed ellipses are plotted according to the parameters listed in BF. Between the mid Bay station 83 and the upper Bay station 140, the tide makes rectilinear motion in the direction aligned with the center axis of the Chesapeake Bay while the current speed is primarily controlled by the width of the channel cross sections. The 3D model appears to have captured these variations of tidal current's magnitude and orientation. In the lower bay stations 79 to 41, the observed tidal ellipses are well reproduced in the 3Ds model, but the

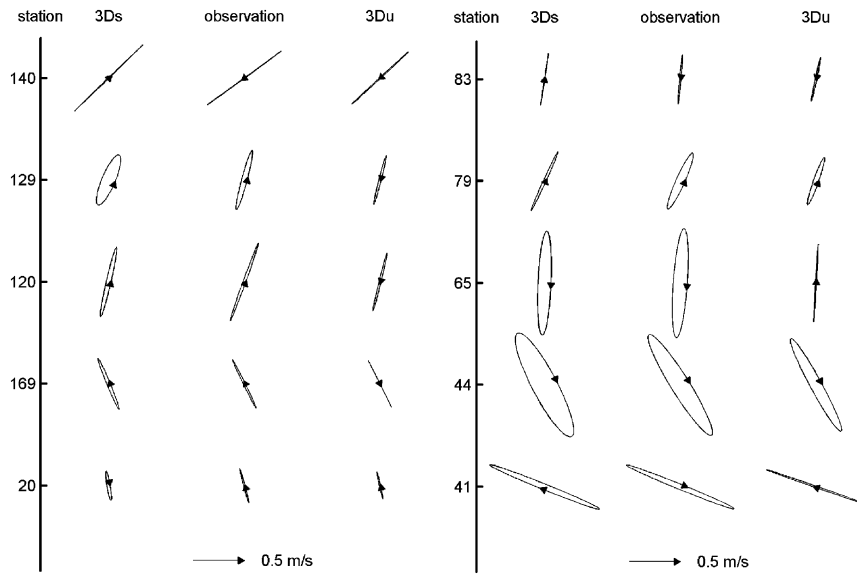


Fig. 8. Comparison of the M_2 current ellipses at 5m depth at 10 current meter stations (see Fig. 1c for the locations) between the observation and models. Arrows in the ellipses denote the sense of rotation.

Table 2

Comparison of the observed and modeled M_2 tidal current ellipse parameters at ten current meter stations (see Fig. 1c for the locations). Positive (Negative) semi-minor means the ellipse rotates in the anticlockwise (clockwise) sense

Station	Semi-major (cm/s)			Semi-minor (cm/s)			Inclination (degree)			Phase (degree)		
	Obs	3Ds	3Du	Obs	3Ds	3Du	Obs	3Ds	3Du	Obs	3Ds	3Du
140	44.6	46.7	37.7	-0.1	0.5	-0.4	36.0	44.1	42.7	200	155	147
129	30.1	26.7	24.9	2.8	6.6	-1.0	75.0	67.0	75.8	168	122	126
120	40.5	35.1	28.9	1.4	2.4	-0.9	70.0	77.0	76.3	132	127	105
169	26.6	27.2	25.5	0.9	1.7	0.1	116.0	112.5	116.5	73	78	72
20	17.5	14.6	13.6	0.7	-1.5	0.7	105.0	99.4	102.5	36	32	29
83	24.1	25.6	22.0	-0.6	0.2	-0.7	85.0	81.3	78.0	342	343	341
79	30.1	32.0	24.8	4.3	1.3	2.5	66.0	65.4	70.4	308	308	300
65	53.5	50.9	38.1	-6.8	-6.3	0.5	86.0	87.5	86.7	308	313	298
44	58.0	57.1	51.5	-8.8	-12.1	-5.6	122.0	117.8	118.5	256	276	267
41	56.7	57.9	51.5	-2.5	-2.8	-0.7	158.0	158.1	161.0	258	267	257

Obs stands for observations, 3Ds for a 3D baroclinic model that includes stratification and 3Du for a 3D model with constant density everywhere.

eccentricity in 3Du model is appreciably weaker, particularly at stations 65, 44 and 41.

We can quantify the predictive skill of tidal currents by carrying out statistical analysis similar to that for the sea level heights. A constituent tidal-current ellipse has five parameters: the semi-major axis, the semi-minor axis, the direction of rotation of the constituent current, the inclination of the semi-major axis of the ellipse, and Greenwich phase lag. The inclination or orientation of an ellipse is

defined to be the angle of semi-major axis measured anticlockwise from the east direction, and its value falls between 0° and 180° . We assign the semi-minor axis a positive (negative) sign when the ellipse rotates in the anticlockwise (clockwise) direction. Table 2 lists a comparison of semi-major, semi-minor, inclination and phase between the data and model results. The rms differences for the 3Ds model are 2.6 , 2.1 cm s^{-1} , 5.1° and 21.7° for the semi-major, semi-minor axes, inclination and phase of the

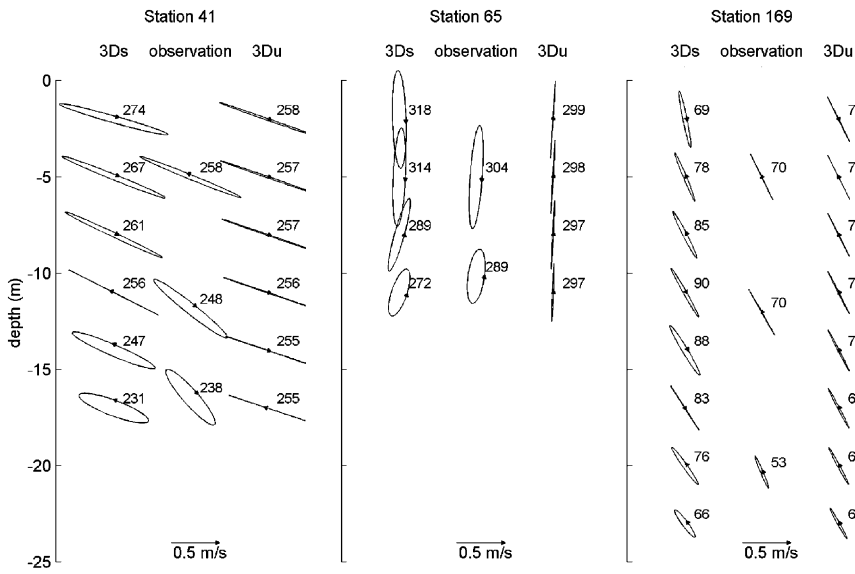


Fig. 9. Comparison of the variation of the M_2 current ellipses with depth at three current-meter stations (see Fig. 1c for the locations). The numbers marked on the ellipses are phase values.

ellipses at these stations, respectively. The rms differences for the 3Du model are 7.5 , 3.0 cm s^{-1} , 4.3° and 23.7° for the semi-major, semi-minor axes, inclination and phase of the ellipses at these stations, respectively. The phase differences are noticeably larger at stations 140 and 129 than at other stations. We think that the discrepancy at these two upper bay stations might be due to their close proximity to the open boundary at the head of the estuary. Specifying tides in addition to the river discharges will likely reduce the discrepancy, but we do not have the observational data to specify tides at this location.

Next we examine variations of tidal currents in the vertical direction, which is shown in Fig. 9. At station 41 at the Bay’s mouth, the tidal currents were measured at three depths and all showed elliptical shapes. The unstratified 3Du run shows rectilinear motion at all depths. The stratified 3Ds run shows elliptical shapes and is in better agreement with the observed ellipses. At Station 65 located between York and Rappahannock River, the data and stratified run both show elliptic shapes whereas the unstratified run does not. At the mid Bay stations 169, both models show good agreement with the observations, although the stratified run shows an eccentricity larger than the observed ones. Overall, the 3Ds model which incorporates the stratification effect does a better job in predicting the vertical variation of tidal current ellipses.

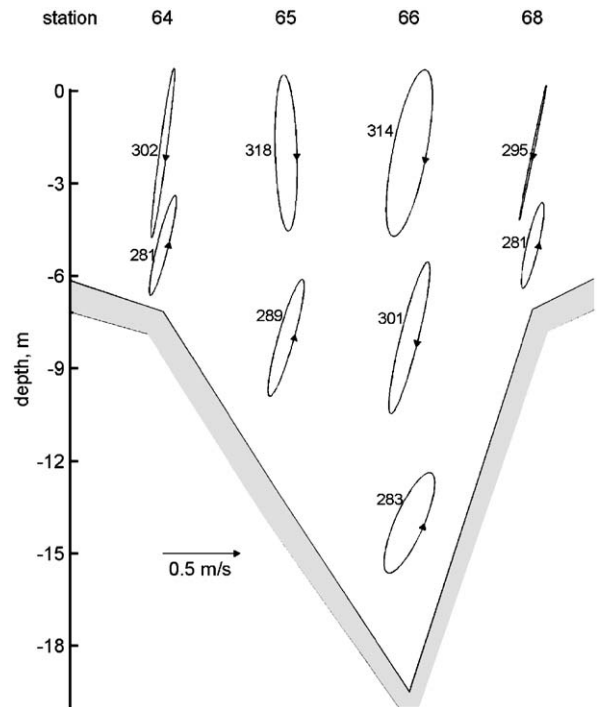


Fig. 10. Model-predicted vertical distribution of the M_2 current ellipses along a lower Bay transect (see Fig. 1c for the locations). The numbers marked on the ellipses are phase values.

Fig. 10 presents the model-predicted tidal current ellipses at four stations along a transect in the lower bay, which was called Wolf Trap light current

station transect in BF (see Fig. 1c). The phase for each current ellipse is marked by a number besides the ellipse. Phase differences are found not only between different water depths at a single station but also between the shallow shoal and deep channel regions. For example, at station 66 located in the deep channel, the phase at 2 m depth is 31° larger than that near the bed, which means that the near-bottom current leads the near-surface current by about 1 h. Such a phase difference was observed in the Chesapeake Bay by BF and in many other coastal oceans (Soulsby, 1983). When the water depth is deeper than the height of the bottom boundary layer, inertial force becomes comparable with or greater than frictional force away from the bottom boundary, causing the current high up in the water column to lag behind those near the bottom. Similarly, stronger friction causes the current in the shallow shoal water to lead that in the deep channel, as shown by the phase differences between the four stations at the 2 m depth. In contrast, the phases at the bottom boundary are about the same everywhere. Besides the phase lags across the channel, semi-major axis length, eccentricity and rotation of the ellipses also vary from the water surface to the bottom.

5. Tidal energy flux and dissipation

Tides in semi-enclosed areas, such as the Chesapeake Bay, are determined primarily by co-oscillation with tidal waves propagating in a neighboring ocean. The direct effect of the tidal-generating force is small and is not considered in this paper. Hence the tides in the Chesapeake Bay derive most of its energy from the oceanic tide at the Bay's entrance. In the previous two sections, we have shown that the 3D baroclinic (3Ds) model can accurately simulate tidal elevations and tidal currents in the Chesapeake Bay. In this section, we shall use the 3Ds model to calculate the amount of the tidal energy flux entering the Bay's mouth and estimate the amount of the energy dissipated inside the Bay. In particular, we will identify regions of enhanced energy dissipation as they are important to the salt transport and maintenance of estuarine circulation in the Chesapeake Bay.

A detailed description of energy flux and energy dissipation calculations is provided in Appendix B. In Figs. 11a and 11b, we examine the distributions of depth-integrated energy flux vectors for the principal semidiurnal M_2 and diurnal K_1 constituents. The spatial distributions of the two vector fields are very

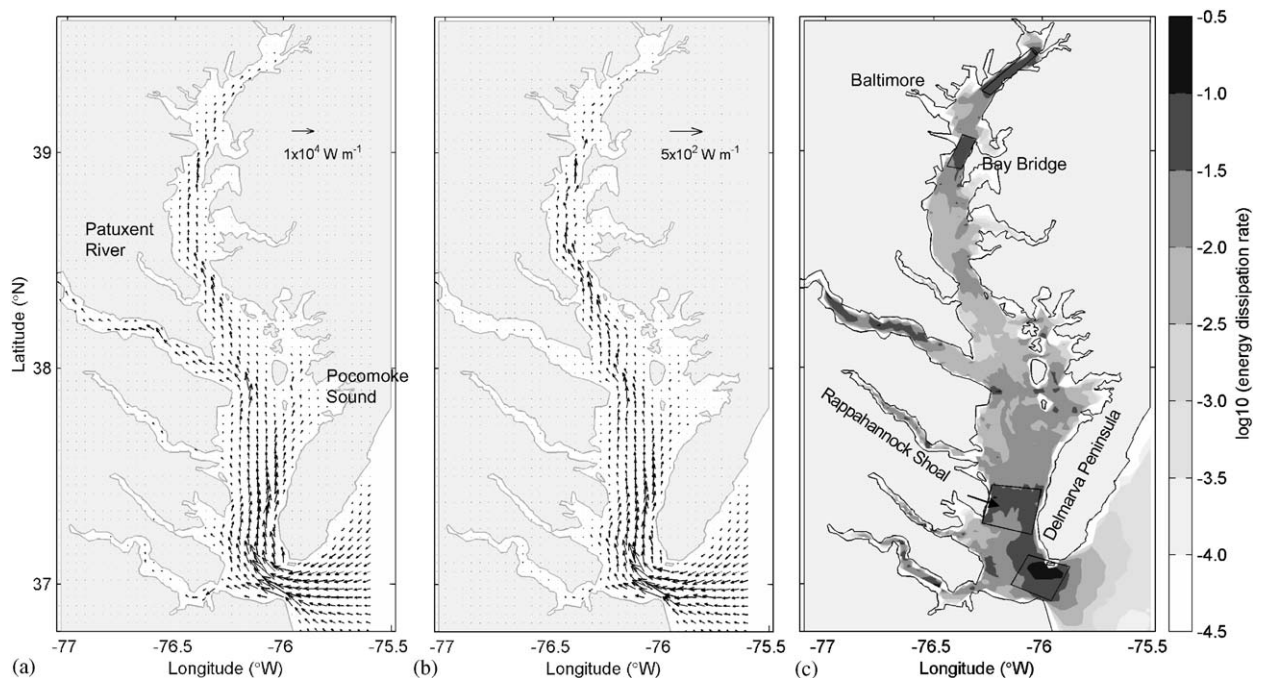


Fig. 11. Depth-integrated barotropic energy flux vectors for M_2 (a), K_1 (b) constituents, and distribution of energy dissipation rate per unit area (c).

similar, but the magnitude of the K_1 flux is much smaller (at least 20 times) than the M_2 flux. Using the M_2 flux as an example, we can follow the pathways of the barotropic tidal energy flux in the Chesapeake Bay. A large incoming tidal energy flux is seen to flow across the Bay's mouth. Some of the tidal energy is delivered to the James and York Rivers connected to the lower Bay, while most of the incoming energy flux is directed northward as the center axis of the main stem Bay turns from an east-west orientation to a south-north direction. The energy flux is higher on the eastern shore, presumably because of the higher tidal range there. North of Rappahannock River, the tidal energy flux is split three ways: one branch into the Potomac River on the western shore, one weaker branch into the Pocomoke Sound area, and the major conduit to deliver tidal energy further north in the main stem. The energy flux vectors are significantly weaker in the upper Bay than in the lower Bay. Near the head of Bay where some tidal waves are reflected, the tidal waves become close to a standing wave so that the net energy flux is small, although the tidal amplitude is enhanced due to the superposition of incoming and reflected waves (see Fig. 5a). The total amount of tidal energy entering the Chesapeake Bay from its adjacent shelf can be estimated by integrating the energy flux across the Bay mouth using Eq. (B.2). The barotropic M_2 energy flux at the Bay-mouth cross section (see Fig. 1c for the location) is calculated to be 165.1 MW ($1\text{MW} = 10^6$ Watts). Energy fluxes from other 4 constituents are 4.6 MW (S_2), 10.5 MW (N_2), 5.0 MW (K_1) and 2.3 MW (O_1), respectively. We have also calculated the energy fluxes from M_4 , M_6 , MS_4 and found them to 0.05, -0.0065 (outward), and 0.0046 MW, respectively. The flux due to the residual Z_0 is -1.8 MW (outward), thus decreasing the total incoming energy flux. Summing the energy fluxes over all these components gives a net flux of 186 MW. If we calculate the energy flux using the original time series of current and pressure and average it over a 58 day period, we get a net flux of 189 MW, which is slightly larger than the value estimated using individual harmonics. Therefore a total of 188 MW tidal energy (excluding that due to Z_0) is pumped into the Chesapeake Bay from its adjacent shelf. We also calculated the M_2 energy flux at other cross-channel sections in the Bay. The energy flux decreases rapidly to about 25 MW at a section near the mouth of Patuxent River. Northward of the Patuxent River, the energy flux decreases more slowly.

To understand why the energy flux changes in this way, we calculate the dissipation of barotropic tidal energy using the formula listed in (B.3) and (B.4). The energy dissipation is highly non-uniform in the Chesapeake Bay, as shown in Fig. 11c. We can identify four hotspots for high energy dissipation.

Hotspot 1 is located around the Bay mouth and appears to be related to the sharp headland formed by the southern tip of the Delmarva Peninsula. As tidal currents move in and out of the Bay mouth, their interaction with the headland generates strong turbulent eddies and results in high energy dissipation. Fig. 12 provides a zoomed-in view of tidal flows in that area. As the ebbing currents rapidly approach the headland, they produce a large eddy, as indicated by high values of vertical vorticity (calculated as the curl of the depth-averaged horizontal velocity vector). Such eddy generation around headlands has been observed in other coastal environments. Signell and Geyer (1991) examined the transient eddy formation around headlands and found that the headland and island eddies in shallow-water are dominated by bottom-friction effects. In deep water, however, both internal tides/waves and baroclinic eddies can generate strong mixing (Pawlak et al., 2003; Edwards et al., 2004). Given the shallow water depth near the Bay's mouth, the headland eddies generated in region 1 are likely controlled by the bottom friction.

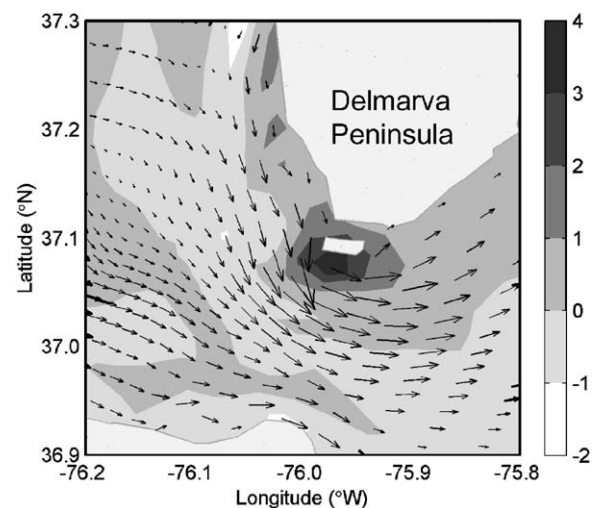


Fig. 12. Depth-averaged current velocity vector (arrows) and vertical vorticity (10^{-4}s^{-1} , gray scale image) during ebb tide, showing eddy generation near the southern tip of Delmarva Peninsula.

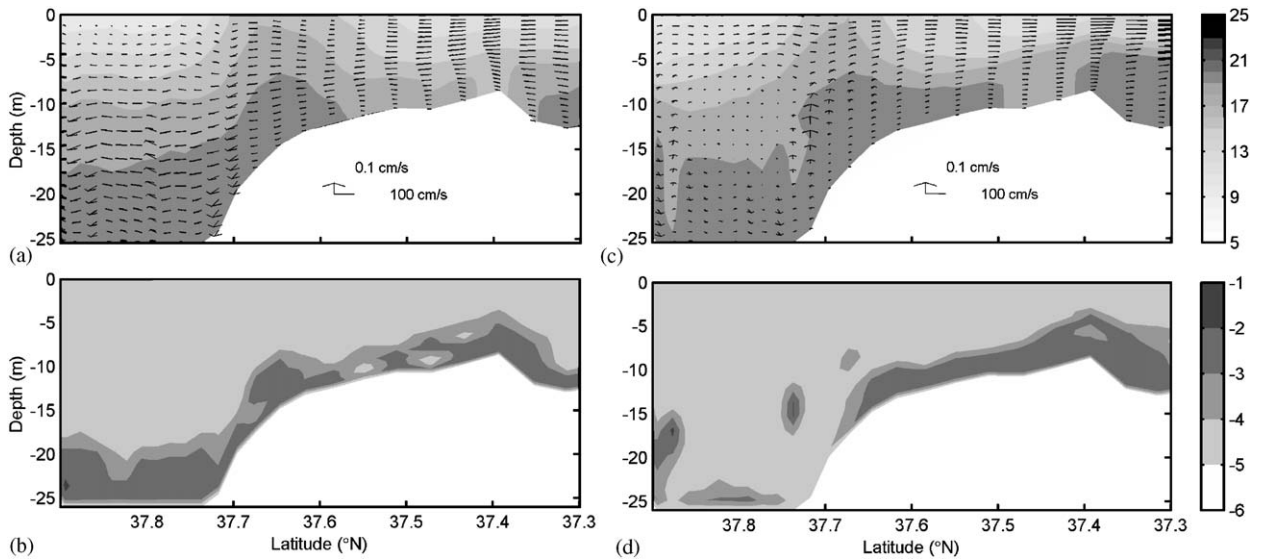


Fig. 13. Distributions of current velocity (arrows) and salinity (contours and gray scale images) around the shallow Rappahannock sill during flood (a) and ebb (c) tide. The \log_{10} of vertical diffusivity ($\text{m}^2 \text{s}^{-1}$) in the same region during flood (b) and ebb (d) tide. Note the velocity scales in horizontal and vertical directions are made different to better visualize the weaker vertical components.

Hotspot 2 is situated near the Rappahannock shoal. Presumably the ebbing currents retreating from the deep mid-Bay channel are pushed up to the shallow regions, generating intense turbulent mixing on their way seaward. Fig. 13 shows the distributions of salinity, current and eddy diffusivity in a vertical section cutting through the Rappahannock sill. Due to the effect of horizontal salinity gradient, the flooding currents show the characteristic subsurface maximum (e.g. Nepf and Geyer, 1996) in the shallow shoal region and dive down the sill as they move further north. Intense turbulent mixing is generated in the bottom boundary layer everywhere. At the ebb phase, the tidal currents accelerate in the shallow shoal regions, producing strong turbulent mixing there. Previous investigations have also shown that sills are sites for enhanced energy dissipation. For example, Freeland and Farmer (1980) calculated the energy lost from the barotropic tide between two pairs of tide gauges in an inlet and found that the majority of the energy was lost in a straight section containing a sill. They hypothesized that the highly turbulent nonlinear lee waves near the sill were responsible for dissipating most of the energy. More recently, Farmer and Armi (1999) found that the small-scale instabilities play a major role in precipitating the strong wake region formed at the downstream side of the

sill. Klymak and Gregg (2004) took extensive dissipation measurements over a tidal cycle and found high energy dissipation rates in the nonlinear lee waves that form each tide over the sill. Our model results are in agreement with these findings and suggest that the shallow sill in the Rappahannock shoal could be a major site of energy sink for the barotropic tidal energy. ROMS model makes hydrostatic approximation and hence cannot simulate non-hydrostatic processes such as nonlinear lee waves that might occur around a sill. The model has a grid size of about 1 km and is not expected to capture detailed turbulent mixing processes in the sill region. Nevertheless, Fig. 13 provides a useful glimpse of local flow patterns around the shallow sill and points to its possible role in regulating salt transport in the entire estuary.

Hotspot 3 is found near the narrow region between the Kent Island and the Western Shore near the Bay Bridge, a topographic constriction. Tidal currents become stronger in the narrower channels and thus produce stronger energy dissipation. Hotspot 4 is located in the very narrow conduit (north of Baltimore) leading up to the head of the Bay, which is also a constriction in the coastlines. Again due to the narrow constriction, the tidal currents become fast and produce relatively strong turbulent mixing there. Hydraulic transitions

near a lateral constriction occur in partially mixed estuaries. A strong front, caused by the hydraulic response of the flow to the constriction at the George Washington Bridge, has been observed during the ebb in the southern portion of the Hudson River estuary (Chant & Wilson, 2000). Enhanced shears in this frontal zone are a source of intensified mixing. Geyer and Smith (1987) mapped the spatial structure of the interfacial mixing processes in a series of longitudinal transects with echo sounder. They observed the plume-like structures that occur at various constriction points along the estuary, suggesting intensification of vertical mixing. The enhanced dissipation of barotropic tidal energy in hotspots 3 and 4 are likely associated with similar mechanism identified above.

Integration of the energy dissipation terms as shown in (B.3) and (B.4) over the whole Bay amounts to 172 MW. We have also calculated energy dissipation due to the horizontal diffusion (see (B.5)) and found it to be 8.3 MW. Thus the total energy dissipation inside the Bay is 180 MW, which is 6 MW less than the net incoming energy flux (incoming tidal flux of 188 MW minus 1.8 MW outflux due to the residual Z_0). This discrepancy amounts to be about 3% error and may be due to the inaccuracy in the numerical computation of velocity derivatives in the energy dissipation terms.

A remarkable feature in Fig. 11c is that large energy dissipation occurs in the lower bay. The combined dissipation rate in hotspots 1 and 2 is about 56 MW and amounts to about 32% of the total energy dissipation in the Chesapeake Bay. Such high dissipation leads to a rapid reduction of tidal height and tidal current speed between the Bay mouth and mid Bay, as shown in Figs. 4a, 5a and 6a. Although the depth-integrated dissipation rate per unit area is relatively high in hotspots 3 and 4 in the upper Bay, the integrated dissipation is only about 8% of the total dissipation because of its small area size.

6. Discussion and conclusion

Using a 3D baroclinic model validated against observed tidal elevations and currents, we calculate the amount of tidal energy flux entering Bay to be 188 MW. How does this compare with the amount of mechanical energy input due to wind? To get a handle on this question, we have carried out a simple calculation using the approach which Lueck and Reid (1984) developed for global oceans. More

recently, Wang and Huang (2004a, b) extended this approach to investigate wind energy inputs to individual components such as the surface Ekman Layer and surface waves. Here we only seek an estimate for the total wind energy input into the Chesapeake Bay. The wind energy input consists of two major parts: one associated with the surface drift and one due to pressure work. Richman and Garrett (1977) examined the rate of wind energy input in the presence of surface waves and suggested that the wind energy input is approximately $0.1\tau U_w$, where τ is the wind stress at the sea surface and U_w is the wind speed at 10-m height. Observations of the surface drift range between 2% and 7% of the 10 m wind speed at angles ranging from 0 to 45 from the wind direction. Accordingly a lower bound for the wind energy input is $0.02\tau U_w$. Hence the wind energy input lies in the range between $0.02\tau U_w$ and $0.1\tau U_w$. We will consider the wind directions and parameterize the wind stress through a drag law

$$\vec{\tau}_w = C_D \rho_a \left(U_{wx}^2 \vec{i} + U_{wy}^2 \vec{j} \right),$$

where U_{wx} and U_{wy} are wind speed components in the east-west and south-north directions, C_D is the drag coefficient and ρ_a the air density.

The total wind energy input to the Chesapeake Bay is thus the integral of ($0.02\tau U_w$ and $0.1\tau U_w$) over the Bay surface. Since the wind field over the Chesapeake Bay is influenced by seasonal weather patterns, we average the wind energy input over a year to obtain the annually averaged wind energy input

$$P_{\text{wind}} = \frac{1}{T_{\text{year}}} \int_0^{T_{\text{year}}} dt \iint (0.02-0.1) \vec{\tau}_w \cdot \vec{U}_w dx dy.$$

Using wind records obtained at three airports in the Chesapeake Bay region and extrapolating them over to the Bay surface, we estimate the wind energy flux P_{wind} to be (27–135) MW if the original airport winds are used but (93–465) MW if the empirical amplification factors are used to account for land-sea differences (Xu et al., 2002).

We also try to estimate the wind energy flux using another approach. Li et al. (2006) coupled the hydrodynamic model with a regional atmosphere model (MM5). Using the wind stress from MM5 and the surface water velocity from ROMS (tidal velocity components were removed through

a low-pass filter), we have calculated the wind energy flux into Chesapeake Bay during a two month period (August and September of 2003). The time-averaged wind energy flux is 103 MW or 66 MW if Hurricane Isabel which hit Chesapeake Bay in September 2003 is excluded. We must remark that these calculations also have limitations because the winds over Chesapeake Bay show strong seasonal variations. Unfortunately we do not have the atmospheric forcing data to do a one-year calculation. We may pursue such calculations in the future.

Based on these calculations, we find that the wind energy input is in the same order of magnitude as the tidal energy flux in the Chesapeake Bay. Although tidal forcing dominates in many estuaries, tidal and wind forcing appear to have nearly equal importance in the Chesapeake Bay. In the deep ocean, Munk and Wunsch (1998) proposed that tidal mixing and wind mixing are equally important, each contributing about one half of the mixing energy required to maintain the global abyssal density distribution. Vertical mixing in the deep ocean leads to a diffuse thermohaline and a much larger meridional heat transport in thermohaline circulation than that without mixing. Similarly, in a partially mixed estuary, turbulent mixing results in a two-layer circulation with volume transports much greater than the river runoff. Investigations into simpler semi-enclosed estuaries may produce helpful hints about processes in the more complex deep ocean. Our simple analysis above suggests that the Chesapeake Bay may be an interesting site for investigating the relative roles of wind and tidal mixing in the ocean.

Given the uncertainty in the wind field and the wide range of wind energy flux in our estimate, we caution that further investigations are needed to obtain an accurate estimate of the wind energy flux. Observations have shown that the wind-driven current is the largest component in the subtidal velocity, suggesting that wind is an important source of mechanic energy into the Bay (Wang, 1979a, b). Wind events have been observed to cause dramatic changes in the salinity distribution, sometimes transforming the partially mixed estuary into a vertically homogeneous estuary (Goodrich et al., 1987). While tide is cyclic and varies over a spring-neap cycle, wind is episodic and responds to seasonal changes in synoptic weather patterns. Turbulent flows generated by tide and wind have dramatically different temporal and spatial char-

acteristics. Therefore, further research into the relative roles of wind and tidal forcing in the Chesapeake Bay is warranted.

In coastal plain estuary such as the Chesapeake Bay, the theoretical framework for the estuarine dynamics is based on the interplay between fresh water input from rivers and turbulent mixing in the bottom boundary layer. However, our calculations have shown that turbulent mixing is highly non-uniform in the Chesapeake Bay. 40% of the total energy dissipation is concentrated in the four hotspots: headland at the Bay mouth, the Rappahannock sill, constrictions at the Bay Bridge and in the upper Bay. Thus an improved understanding of estuarine circulation in the Chesapeake Bay requires better understanding of topographically controlled mixing in these hotspots of high energy dissipation.

Acknowledgements

We thank NOAA for providing sea level data at tidal gauges. This work is supported by grants from NOAA/CICEET and NSF. We thank Mike Foreman and one anonymous referee for helpful comments. This is UMCES contribution 3925.

Appendix A. Definitions of statistical quantities for error analysis

To quantify the predictive skill of tidal models, we compute the following statistical measures: the root-mean-square (rms) error

$$rms = \left\{ \frac{1}{N} \sum_{i=1}^N (\eta_{\text{mod}} - \eta_{\text{obs}})^2 \right\}^{1/2}, \quad (\text{A.1})$$

the relative average error (E)

$$E = 100\% \frac{\sum_{i=1}^N (\eta_{\text{mod}} - \eta_{\text{obs}})^2}{\sum_{i=1}^N (|\eta_{\text{mod}} - \bar{\eta}_{\text{obs}}|^2 + |\eta_{\text{obs}} - \bar{\eta}_{\text{obs}}|^2)}, \quad (\text{A.2})$$

and the correlation coefficient

$$r = \frac{\sum_{i=1}^N (\eta_{\text{mod}} - \bar{\eta}_{\text{mod}})(\eta_{\text{obs}} - \bar{\eta}_{\text{obs}})}{\left[\sum_{i=1}^N (\eta_{\text{mod}} - \bar{\eta}_{\text{mod}})^2 \sum_{i=1}^N (\eta_{\text{obs}} - \bar{\eta}_{\text{obs}})^2 \right]^{1/2}}, \quad (\text{A.3})$$

following Spitz and Klinck (1998). We also examine a model skill parameter used by Warner et al. (2005b) in their simulations of the Hudson River estuary,

$$Skill = 1 - \frac{\sum_{i=1}^N |\eta_{\text{mod}} - \eta_{\text{obs}}|^2}{\sum_{i=1}^N (|\eta_{\text{mod}} - \bar{\eta}_{\text{obs}}| + |\eta_{\text{obs}} - \bar{\eta}_{\text{obs}}|)^2}, \quad (\text{A.4})$$

where η is the variable being compared, $\bar{\eta}$ its time mean, and the subscripts mod and obs stand for model results and observations, respectively. Perfect agreement between the model results and observations yields a skill of 1.0 whereas complete disagreement yields a skill of 0.

For a tidal constituent at a measurement station, the root-mean-square (rms) difference between the model and observations, D , is calculated according to

$$D = \sqrt{\frac{1}{2}(A_{\text{obs}}^2 + A_{\text{mod}}^2) - A_o A_m \cos(\phi_{\text{obs}} - \phi_{\text{mod}})}, \quad (\text{A.5})$$

where A , ϕ are amplitudes and phases for the constituent, respectively (see Cummins and Oey, 1997; Cummins et al., 2000).

Appendix B. Calculation of energy fluxes and energy dissipation

Integration of the energy equation for the horizontal velocities (Gill, 1982) over a control volume V bounded by surface S and averaging over a tidal cycle yields

$$\begin{aligned} & \iint \left\langle \left(p + \rho_0 \frac{u^2 + v^2}{2} \right) \vec{u} \cdot \vec{n} \right\rangle dS \\ &= \iiint \rho_0 \left\langle \left[\frac{\partial}{\partial z} \left(u K_V \frac{\partial u}{\partial z} \right) + \frac{\partial}{\partial z} \left(v K_V \frac{\partial v}{\partial z} \right) \right] \right. \\ & \quad \left. - K_V \left[\left(\frac{\partial u}{\partial z} \right)^2 + \left(\frac{\partial v}{\partial z} \right)^2 \right] \right\rangle dV + Diss_h \end{aligned} \quad (\text{B.1})$$

where the angle brackets denote the tidal average and $Diss_h$ represents the dissipation due to horizontal diffusion (see (B.5)). This equation states a balance between the mean energy fluxes normal to the volume surface (left hand side term, e.g., through the open boundaries of the Chesapeake Bay) and the mean energy dissipation (right-hand

side terms). We shall consider only the energy flux due to the work done by the pressure force associated with barotropic tidal motion. The advective contribution to the energy flux (i.e., the second term in left-hand side of the above equation) is usually two orders of magnitude smaller than the barotropic flux and hence will be neglected. Therefore, the depth-integrated energy flux per unit length can be computed according to

$$\vec{F} = \rho_0 g H \langle \vec{u} \eta \rangle, \quad (\text{B.2})$$

where H is the water depth, \vec{u} the depth-averaged velocity and η sea level fluctuation. The depth-integrated energy flux for a specified tidal constituent can be calculated through its harmonic constants of tidal elevation and velocity (see Cummins and Oey, 1997). The total energy flux is then the sum of fluxes for each individual constituent. In general the energy flux is proportional to the square of the tidal amplitude as tidal current is proportional to the tidal amplitude. Given that the amplitudes of S_2 , N_2 , K_1 and O_1 tides are small compared to M_2 , their combined contribution to the energy flux is only about 10% of the M_2 flux.

Dissipation of barotropic tidal energy in the right-hand side of Eq. (B.1) contains three parts, of which the first term can be further simplified as

$$\begin{aligned} & \iiint \rho_0 \left\langle \frac{\partial}{\partial z} \left(u K_V \frac{\partial u}{\partial z} \right) + \frac{\partial}{\partial z} \left(v K_V \frac{\partial v}{\partial z} \right) \right\rangle dV \\ &= \iint \langle \vec{u}_s \cdot \vec{\tau}_s - \vec{u}_b \cdot \vec{\tau}_b \rangle dS \\ &= - \iint \rho_0 C_D \langle |\vec{u}_b|^3 \rangle dS, \end{aligned} \quad (\text{B.3})$$

where zero surface stress (no wind) and quadratic drag coefficient at the bottom has been applied. The cubic law of energy dissipation implies that magnitude of energy dissipation integrated over a specified area will depend mostly on a few spaces where the currents are greatest. We calculate the bottom velocity at a specified depth, say 1 m above the bottom at each water grid point, and then average its cubic power over 58 days which is an integer number of periods for each of the major constituents. This term represents the dissipation of barotropic tidal energy and the production of turbulent kinetic energy in the bottom log layer.

The second part of energy dissipation in Eq. (B.1) is calculated as

$$-\iiint \rho_0 \left\langle K_V \left[\left(\frac{\partial u}{\partial z} \right)^2 + \left(\frac{\partial v}{\partial z} \right)^2 \right] \right\rangle dV = -\iint \left\{ \frac{1}{T} \int_0^T \rho_0 \int_{-H}^{\eta} K_V \left[\left(\frac{\partial u}{\partial z} \right)^2 + \left(\frac{\partial v}{\partial z} \right)^2 \right] dz dt \right\} dS. \quad (\text{B.4})$$

At each water grid point, we first integrate dissipation rate over the water column, and then average it over 58 days.

The third part Diss_h is related to the dissipation of barotropic tidal energy by horizontal diffusion and can be simplified to

$$-\iiint \rho_0 \left\langle K_H \left[\left(\frac{\partial u}{\partial x} \right)^2 + \left(\frac{\partial u}{\partial y} \right)^2 + \left(\frac{\partial v}{\partial x} \right)^2 + \left(\frac{\partial v}{\partial y} \right)^2 \right] \right\rangle dV. \quad (\text{B.5})$$

This term is calculated using the same numerical approach as (B.4).

References

- Browne, D.R., Fisher, C.W., 1988. Tide and tidal currents in the Chesapeake Bay. NOAA Technical Report NOS OMA 3.
- Carbajal, N., Backhaus, J.O., 1998. Simulation of tides, residual flow and energy budget in the Gulf of California. *Oceanologica Acta* 21 (3), 429–446.
- Carter, H.H., Pritchard, D.W., 1988. Oceanography of Chesapeake Bay. In: Kjerfve, B. (Ed.), *Hydrodynamics of Estuaries: Dynamics of Partially Mixed Estuaries*, vol. 1. CRC Press, Boca Raton FL, pp. 1–16.
- Chant, R.J., Wilson, R.E., 2000. Internal hydraulics and mixing in a highly stratified estuary. *Journal of Geophysical Oceanography* 105 (C6), 14215–14222.
- Cummins, P.F., Oey, L.Y., 1997. Simulation of barotropic and baroclinic tides off Northern British Columbia. *Journal of Physical Oceanography* 27 (5), 762–781.
- Cummins, P.F., Masson, D., Foreman, M.G.G., 2000. Stratification and mean flow effects on diurnal tidal currents off Vancouver Island. *Journal of Physical Oceanography* 30, 15–30.
- Daily, J.W., Harleman, D.R.F., 1966. *Fluid Dynamics*. Addison-Wesley, Reading, MA, pp. 297–298.
- Davies, A.M., Kwong, S.C.M., 2000. Tidal energy fluxes and dissipation on the European continental shelf. *Journal of Geophysical Research* 105 (C9), 21969–21989.
- Edwards, K.A., MacCready, P., Moun, J.N., Pawlak, G., Klymak J. M., Perlin A., 2004. Form drag and mixing due to tidal flow past a sharp point. *Journal of Physical Oceanography* 34, 1297–1312.
- Egbert, G.D., Erofeeva, S.Y., 2002. Efficient inverse modeling of barotropic ocean tides. *Journal of Atmospheric and Oceanic Technology* 19 (2), 183–204.
- Egbert, G.D., Bennett, A., Foreman, M., 1994. TOPEX/Poseidon tides estimated using a global inverse model. *Journal of Geophysical Research* 99 (C12), 24821–24852.
- Farmer, D., Armi, L., 1999. Stratified flow over topography: the role of small-scale entrainment and mixing in flow establishment. *Proceedings of the Royal Society of London Series A* 455, 3221–3258.
- Foreman, M.G.G., Sutherland, G., Cummins, P.F., 2004. M_2 tidal dissipation around Vancouver Island: an inverse approach. *Continental Shelf Research* 24 (18), 2167–2185.
- Freeland, H.J., Farmer, D.M., 1980. Circulation and energetics of a deep, strongly stratified inlet. *Canadian Journal of Fisheries and Aquatic Sciences* 37, 1398–1410.
- Geyer, W.R., Smith, J.D., 1987. Shear instability in a highly stratified estuary. *Journal of Physical Oceanography* 17, 1668–1679.
- Gill, A.E., 1982. *Atmosphere-Ocean Dynamics*. Academic Press, New York 662 pp.
- Goodrich, D.M., Boicourt, W.C., Hamilton, P., Pritchard, D.W., 1987. Wind-induced destratification in Chesapeake Bay. *Journal of Physical Oceanography* 17, 2232–2240.
- He, R., Weisberg, R.H., 2002. Tides on the West Florida Shelf. *Journal of Physical Oceanography* 32 (12), 3455–3473.
- Hicks, S.D., 1964. Tidal wave characteristics of Chesapeake Bay. *Chesapeake Science* 5, 103–113.
- Klymak, J.M., Gregg, M.C., 2004. Tidally generated turbulence over the knight inlet sill. *Journal of Physical Oceanography* 34, 1135–1151.
- Lavelle, J.W., Mofjeld, H.O., Lempriere-doggett, E., Cannon, G.A., Pashinski, D.J., Cokelet, E.D., Lytle, L., Gill, S., 1988. A multiply connected channel model of tides and tidal currents in puget sound; Washington and a comparison with updated observations. NOAA Tech. Memo. ERL PMEL-84; Pacific marine environmental laboratory; NOAA.
- Levitus, S., 1982. *Climatological atlas of the world ocean*. NOAA Prof. Pap. 13. US Govt. Print Off, Washington DC 173 pp.
- Li, M., Zhong, L., Boicourt, W.C., 2005. Simulations of Chesapeake Bay estuary: sensitivity to turbulence mixing parameterizations and comparison with observations. *Journal of Geophysical Research* 110, C12004.
- Li, M., Zhong, L., Boicourt, W.C., Zhang, S., Zhang, D.-L., 2006. Hurricane-induced storm surges, currents and destratification in a semi-enclosed bay. *Geophysical Research Letters* 33, L02604.
- Lueck, R., Reid, R., 1984. On the production and dissipation of mechanical energy in the ocean. *Journal of Geophysical Research* 89 (C3), 3439–3445.
- Munk, W., 1997. Once again: once again—tidal friction. *Progress Oceanography* 40, 7–35.
- Munk, W., Wunsch, C., 1998. Abyssal recipes II: energetics of tidal and wind mixing. *Deep-Sea Research I* 45, 1977–2010.

- Nepf, H.M., Geyer, W.R., 1996. Intratidal variations in stratification and mixing in the Hudson estuary. *Journal of Geophysical Research* 101, 12079–12086.
- Pawlak, G., MacCready, P., Edwards, K. A., McCabe, R., 2003. Observations on the evolution of tidal vorticity at a stratified deep water headland. *Geophysical Research Letters* 20(24), 2234, doi:10.1029/2003GL018092.
- Pawlowicz, R., Beardsley, B., Lentz, S., 2002. Classical tidal harmonic analysis including error estimates in MATLAB using T_TIDE. *Computers and Geosciences* 28, 929–937.
- Richman, J., Garrett, C., 1977. The transfer of energy and momentum by the wind to the surface mixed layer. *Journal of Physical Oceanography* 7, 876–881.
- Sheng, J., Wang, L., 2004. Numerical study of tidal circulation and nonlinear dynamics in Lunenburg Bay, Nova Scotia. *Journal of Geophysical Research* 109, C10018, doi:10.1029/2004JC002404.
- Song, Y.T., Haidvogel, D.B., 1994. A semi-implicit ocean circulation model using a generalized topography-following coordinate. *Journal of Computation Physics* 115, 228–244.
- Soulsby, R.L., 1983. The bottom boundary layer of shelf seas. In: John, B. (Ed.), *Physical Oceanography of Coastal and Shelf Seas*. Elsevier, Amsterdam, pp. 189–266.
- Signell, R.P., Geyer, W.R., 1991. Transient eddy formation around headlands. *Journal of Geophysical Research* 96 (C2), 2561–2575.
- Spitz, Y.H., Klinck, J.M., 1998. Estimate of bottom and surface stress during a spring-neap tide cycle by dynamic assimilation of tid gauge observations in the Chesapeake Bay. *Journal of Geophysical Research* 103 (C6), 12761–12782.
- Tinis, S.W., Pond, S., 2001. Tidal Energy Dissipation at the Sill of Sechart Inlet, British Columbia. *Journal of Physical Oceanography* 31 (12), 3365–3373.
- Wang, D.-P., 1979a. Subtidal sea level variations in the Chesapeake Bay and relation to atmospheric forcing. *Journal of Physical Oceanography* 9, 413–421.
- Wang, D.-P., 1979b. Wind-driven circulation in the Chesapeake Bay, winter 1975. *Journal of Physical Oceanography* 9, 564–572.
- Wang, W., Huang, R.X., 2004a. Wind energy input to the Ekman layer. *Journal of Physical Oceanography* 34 (5), 1267–1275.
- Wang, W., Huang, R.X., 2004b. Wind energy input to the surface waves. *Journal of Physical Oceanography* 34 (5), 1276–1280.
- Warner, J.C., Sherwood, C.R., Arango, H.G., Butman, B., Signell, R.P., 2005a. Performance of four turbulence closure models implemented using a generic length scale method. *Ocean Modeling* 8, 81–113.
- Warner, J.C., Geyer, W.R., Lerczak, J.A., 2005b. Numerical modeling of an estuary: a comprehensive skill assessment. *Journal of Geophysical Research* 110, C05001, doi:10.1029/2004JC002691.
- Xu, J., Chao, S.Y., Hood, R.R., Wang, H., Boicourt, W.C., 2002. Assimilating high-resolution salinity data into a model of a partially mixed estuary. *Journal of Geophysical Research* 107 (C7), doi:10.1029/2000JC000626.